FOREX Publication
Open Access | Rapid and quality publishing

International Journal of Electrical and Electronics Research (IJEER)
Research Article | Volume 12, Issue 3 | Pages 827-835 | e-ISSN: 2347-470X

Studying Relative Merits of FOC and DTC for 1-Ø Synchronous Induction Motor Powered by Solar Cell

Nihad Abdulkudhur Jasim[1] and Suha Sabah Shyaa[2*]

[1]*Department of Electrical Power Engineering Techniques/ Technical College Al-Musaib, Al-Furat Al-Awsat Technical University, Najaf, Iraq; nihad.hammoud@atu.edu.iq*
[2]*Department of Electrical Power Engineering Techniques/ Technical College Al-Musaib, Al-Furat Al-Awsat Technical University, Najaf, Iraq; suha.odah@atu.edu.iq*

*__Correspondence:__ Suha Sabah Shyaa; *suha.odah@atu.edu.iq*

ABSTRACT- The paper studies the merits of a 1-Ø induction motor powered by a Trina Solar's module TSM-250PA05.08 that employs the perturbs and observes (P&O) technique, utilizing two types of controllers, FOC and DTC. The merits of the two types of controllers were studied according to the results of the electromagnetic torque (Te), the currents of the main winding Ia and auxiliary winding I_b, and the Speed of a rotor. The results showed that both controllers' electromagnetic torque and speed rotor are very close. The results also showed distortions in the main and auxiliary winding currents when using the DTC controller. In contrast, when utilizing FOC, the results demonstrate smoother waveforms for main and auxiliary winding curves. Regarding response time, DTC achieves a faster rise time for Te and I_b than FOC. Also, concerning settling time, DTC achieves a faster settling time than FOC.

Keywords: Direct Torque; Solar Cell; Induction Motor; Field oriented.

ARTICLE INFORMATION
Author(s): Nihad Abdulkudhur Jasim and Suha Sabah Shyaa;
Received: 21/05/2024; **Accepted**: 16/07/2024; **Published**: 30/07/2024;
e-ISSN: 2347-470X;
Paper Id: IJEER 2105-22;
Citation: 10.37391/IJEER.120313
Webpage-link:
https://ijeer.forexjournal.co.in/archive/volume-12/ijeer-120313.html

crossref member CROSSREF.ORG THE CITATION LINKING BACKBONE

Publisher's Note: FOREX Publication stays neutral with regard to Jurisdictional claims in Published maps and institutional affiliations.

1. INTRODUCTION

The 1-Ø induction motor has recently become one of the most popular AC motors, and it has a wide range of uses, including in household and agricultural products[1][2] . Various control strategies have been introduced for induction machines, such as FOC field control and DTC direct torque control, to increase the performance of induction machines [3] [4]. Both strategies achieved a convergent approach to controlling the induction machine [5]. In the 1980s, an FOC based mainly on the magnetic field of a stator was proposed. In FOC, the AC motor can be controlled by the DC motor's control method, which can control the flux linkage and torque by converting the 3-Ø transform to the 2-Ø perpendicular using the coordinates transformation [6]. Through the mid-1980s, the direct torque control (DTC) algorithm was employed. DTC control strategy cannot achieve rapid and accurate torque control responses without complex algorithms [7]. This algorithm calculates the instantaneous stator flux and torque (stator currents and voltages) based on the key variables [8]. By choosing an ideal inverter switching table, which is utilized to establish the inverter's ideal voltage vector to achieve the fastest torque control and control of stator flux, consider the following structure torque that be achieved instantaneously [8] [9]. DTC structure is simple because it does not require a coordinate transform or a current regulator; therefore, it can be considered a high-performance vector controller based on flux and torque separation [9]. For environmental considerations [10] [11], the *1-Ø* induction motor powered by solar PV is commonly used because environmental degradation is the most serious threat to the planet's health and renewable energy has been widely used to combat it, as solar energy can be used for various applications, including grid network feeding and battery charging [12]. An effective and prominent method for maximizing power harvesting from PV solar is the maximum power point tracking (MPPT) system, which employs the perturb & observe (P&O) technique [13] [14]. The management and operation of a single induction motor driven by standard photovoltaic (PV) cells are examined in this article. There are two ways to regulate the Speed of an induction motor: direct torque control (DTC) and field-oriented control (FOC). The simulation results of the two controllers are contrasted in order to determine whether the strategy has a more substantial effect on the actions of an efficient 1-Ø induction motor drive.

2. THE PROPOSED SYSTEM ARCHITECTURE

The solar converter employed in the suggested system is the H-bridge, as seen in *figure 1*. PV cells might produce electricity. This is achieved by producing electrical energy from solar energy. A DC link voltage is kept constant since an H-bridge transforms a PV array output voltage. Using a rectifier, brake chopper, and an IGBT inverter, a 1-Ø induction motor is operated to help variable speed performance achieve MPPT.

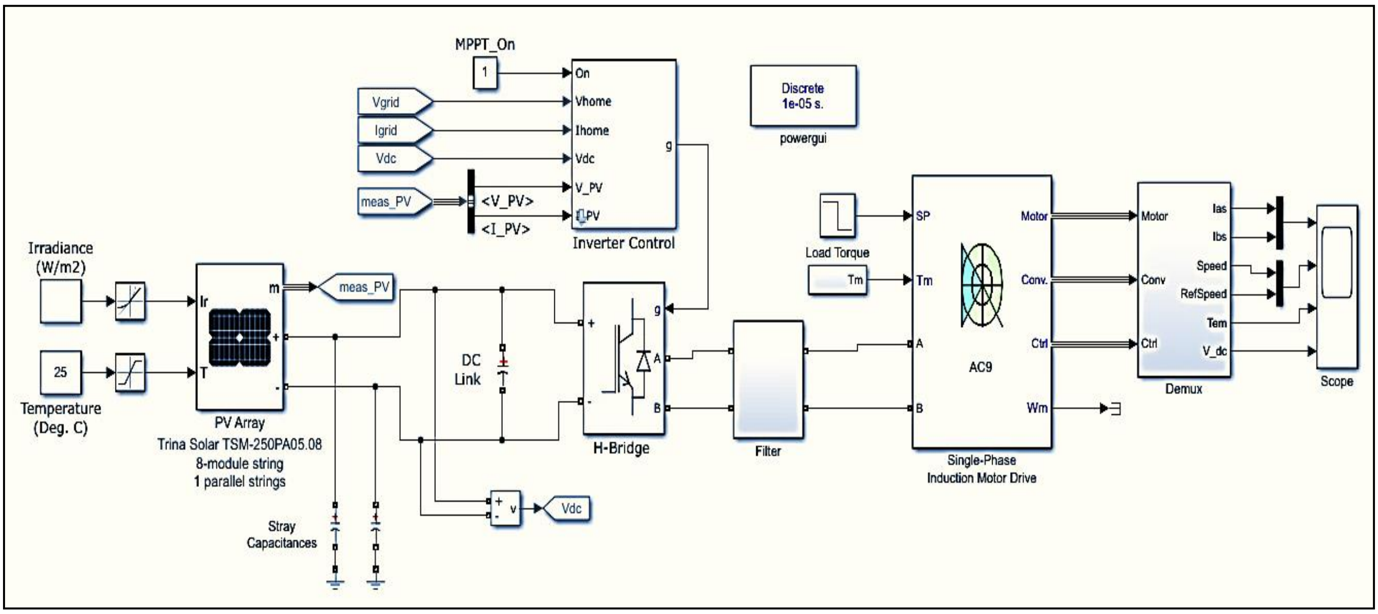

Figure 1. Proposed System Schematic

A 1-Ø induction motor drive is required for a 1/4 HP, 1-Ø AC motor with 110 V and 60 Hz for primary and auxiliary windings machine type. A 1-Ø H-bridge inverter drives an induction motor. An inverter is controlled using PWM, and a speed control loop generates the references for the block controller for both flux and torque. After testing various cell types, the Trina Solar photovoltaic model TSM-250PA05.08 modules were selected. In comparison to other models) compared with Trina Solar TSM-245PD05.081 and Trina Solar TSM-245PD05.08C), the "TSM-250PA05.08" generated the best voltage and current level, according to the comparison findings. The findings of this comparison cannot be discussed in this study.

3. DESIGN CHARACTERISTICS FOR PV ARRAY

The features of the photovoltaic (PV) cell may described using the electrical equivalent circuit, as depicted in *figure 2*. Silicon is a predominant semiconductor material utilized in the construction of solar panels because of its exceptional conductivity control capabilities [15].

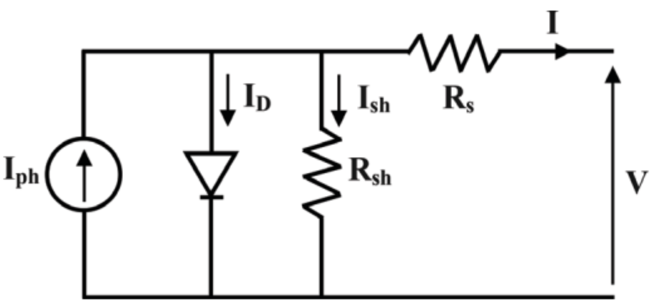

Figure 2. SPV cell design

Sun cells directly convert sun energy into electricity, generating electrical power. A formation of these cells occurs in modules [16], [15]. Several photovoltaic (PV) modules are commonly employed to fulfill various energy requirements [15]. This paper describes the implementation of a Trina Solar TSM-250PA05.08 array module, which consists of the photovoltaic (PV) array created by connecting PV modules in parallel and series. Two inputs on a PV array block permit the temperature and solar irradiance data supply: the input *T* indicates temperature in degrees Celsius, and the input *Ir* indicates irradiance in W/m^2. The PV array comprises a single string of eight Trina Solar TSM-250PA05.08 modules interconnected in series. Under a temperature of 25^o and an irradiation of 1000 Watts per square meter, the string can generate 3486 Watts of power. Minimal capacitors, consisting of two capacitors connected to the terminals of the PV array, are employed to replicate the presence of parasitic capacitance between photovoltaic modules and the ground. The circuit depicted in *figure 2* may expressed using the V-I equation of a Photovoltaic (PV) system as described by *equation (1)* [17] [18].

$$I = Iph - ID * \left(e^{(V+I*Rs)/(N*\,kB\,*T/q)} - 1\right) - \frac{(V+I*Rs)}{Rsh} \quad (1)$$

$$I_{Ph} = Iph_0 * \frac{I_r}{Ir_0}$$

Where: I_{ph}: the current generated by solar radiation, I_r: the amount of light intensity (irradiance) measured in W/m^2, $\mathbf{I_{ph_o}}$: The solar-generated current is measured for the irradiation $\mathbf{I_{r_o}}$. I_D refers to the reverse diode's saturation current. R_s is series resistance & R_{sh} is & shunt resistance, measured in ohms. kB denoted as "Boltzmann constant". *T* represents the value of the temperature parameter used in device simulation. q represents the elementary charge of an electron. *N* represents the ideality factor. *V* represents the voltage across the ports of a solar cell.
PV array specifications are demonstrated in *table 1*.

FOREX Publication
Open Access | Rapid and quality publishing

International Journal of
Electrical and Electronics Research (IJEER)
Research Article | Volume 12, Issue 3 | Pages 827-835 | e-ISSN: 2347-470X

Table 1. Specifications of the PV array

	One module	Array module
Maximum power at MPPT	249.860 Watt	3486.0 Watt
voltage at MPPT	31.0 volt	434.0 volt
current at MPPT	8.060 Amper	8.060 Amper
$V_{o.c}$	37.60 volt	526.40 volt
$I_{s.c}$	8.550 Amper	8.550 Amper
Light-generated current I_L	-	8.57950 Amper
R_{sh}	301.8149 Ω	301.8149 Ω
R_s	0.2470 Ω	1.9760 Ω
number of series modules	--	8
number of parallel modules	--	1

3.1 Perturb & Observe (P&O) Methodology of PV System.

The purpose of MPP tracker use in the PV array is to constantly monitor and adjust the maximum power point (MPP) in response to changes in irradiance and temperature [19].

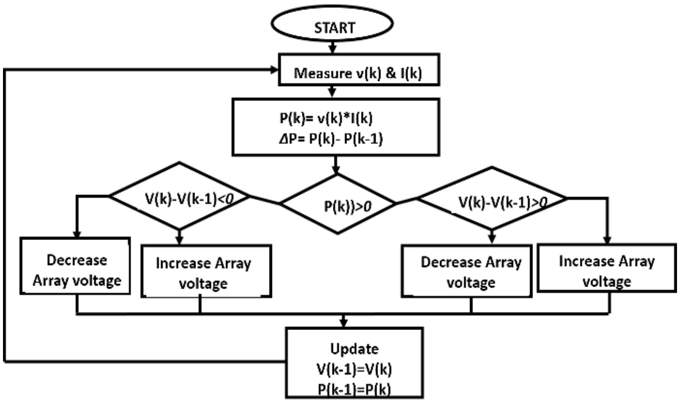

Figure 3. P& O method flow chart

Figure 3 [17] [20] depicts the flowchart that corresponds to the execution of the perturb and observe (P & O) technique. The P & O method intermittently adjusts the panel voltage, comparing the PV output power with that of the preceding cycle. If the disturbance leads to an increase or decrease in the power of the module, the second disturbance happens in the opposite direction. The dimensions of the stride and the duration between iterations of the algorithm are the two elements influencing this approach. The two variables make a trade-off between faster tracking and higher accuracy [19] [21].

4.THE 1-Ø INDUCTION MOTOR

A stator and a rotor, which are the motor's fixed and moveable elements, make up a 1- Ø induction motor, a synchronous alternating current device. The stator in the *1-Ø* induction motor generates an electromagnetic field by using alternating current voltage seeking to synchronize with the stator field a second field emerges because of the current flowing through the rotor as a result of the induced field, maintaining rotation [22] [23]. *Figure 4* depicts the schematic of a 1-Ø induction motor [24] [25].

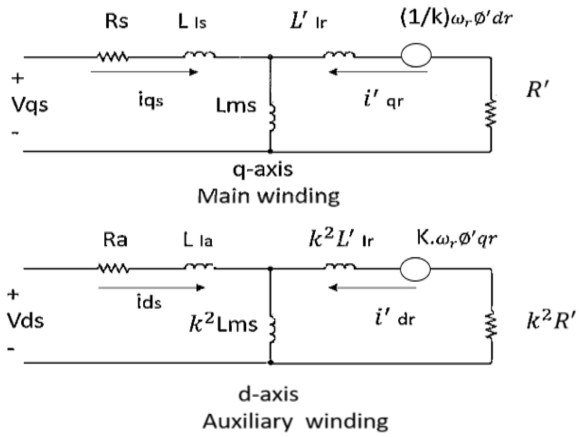

Figure 4. Equivalent Circuit of a Stationary Reference Frame Unsymmetrical 1-Ø Induction Motor

Table 2 shows the ratings of the induction motor.

Table 2. 1- Ø Induction Motor Parameter

Parameter	Unit	Value
Machine Types		Main & Auxiliary Windings
Rating	hp	¼
Voltage	volts	110
Frequency (*f*)	Hz	60
Resistance of the Stator (Main Winding)	Ω	2.02
Inductance of the Stator (Main Winding)	mH	7.4
Mutual inductance	H	0.1772
Resistance of the Stator (Secondary Winding).	Ω	7.14
Inductance of the Stator (Secondary Winding).	mH	8.5
Turn ratio (aux/main)		1.18
Resistance of the Main Winding (Rotor)	Ω	4.12
Inductance of the Main Winding (Rotor)	Mh	5.6
Initial Speed (% Synchronous Speed)		0%

4.1 The 1-Ø Induction Motor with FOC Technique

Advanced control technology called field-oriented control (FOC) measures the Speed of the induction machine. To adapt to changes in online parameters, FOC was built to meet high-performance torque and speed control response needs. A PI controller utilized in FOC creates overshoot and undershoot when there is a load disturbance. Flux and torque are produced for sinusoidally distributed stator windings in alpha-beta frames

Research Article | Volume 12, Issue 3 | Pages 827-835 | e-ISSN: 2347-470X

[1] [26] [27]. The key component of FOC, the rotor flux position θ_s, is determined as follows:

$$\theta_s = \int \omega_S \, dt = \int \left(p \cdot \omega_m + \frac{iq}{Tid} \right) dt \tag{2}$$

Where T is the rotor time constant, ω_m is the rotor speed, and p is the machine pole pairs.

As a result of the rotational change, the $\alpha - \beta$ components to $d - q$ components [28],

$$[D] = \begin{bmatrix} \cos\theta_s & \sin\theta_s \\ \sin\theta_s & \cos\theta_s \end{bmatrix} \tag{3}$$

Where D is the rotational transformation

$$[i_d \; i_q]^T = [D][\, i_\alpha \; i_\beta]^T \tag{4}$$

As i_d and i_q $\alpha - \beta$ components and i_α and i_β are $d - q$ components

In FOC, the following dynamic equations apply to the 1-induction motor when it is under PI vector control [1]:

$$\frac{d}{dt} i_{sd} = -\frac{i_{sd}}{\sigma\tau'_s} + \omega_s i_{sq} + \frac{\emptyset_r}{\sigma L_s \tau_r} + \frac{v_{sd}}{\sigma L_s} \tag{5}$$

$$\frac{d}{dt} \emptyset_r = -\frac{1}{\tau_r} \emptyset_r + \frac{(1-\sigma)L_s}{\tau_r} i_{sd} \tag{6}$$

$$\frac{d}{dt} i_{sq} = -\frac{i_{sq}}{\sigma\tau'_s} - \omega_s i_{sd} + \frac{P}{\sigma L_s} \omega_r \emptyset_r + \frac{v_{sq}}{\sigma L_s} \tag{7}$$

$$\frac{d}{dt} \omega_m = \frac{P}{J} \emptyset_r i_{qs} - \frac{1}{J} T_L \tag{8}$$

where $\emptyset_r$ That would be the direct-axis rotor flux linkage. ω_s is the synchronous angular velocity, $\tau_S{}' = L_S \,/\, R_{seq}$, $\sigma = 1 - M^2 \,/\, L_s L_R$, $R_{Seq} = M^2 \,/\, {L_s}^2$ and $\tau_r = L_r \,/\, R_r$ where, τ_r The time constant of the rotor. 1-Ø induction motor, a breaking chopper, an inverter, and a rectifier made up of a single induction motor drive. The FOC controller generates the gating pulses for the inverter, schematically depicted in *figure 5(a)*. *Figure 5(b)* depicts a flowchart for FOC algorithm.

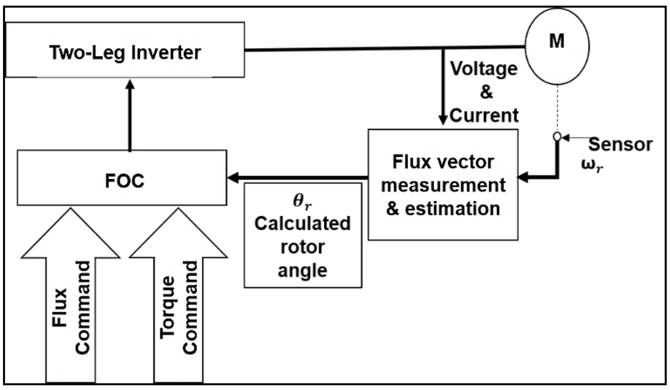

(a)

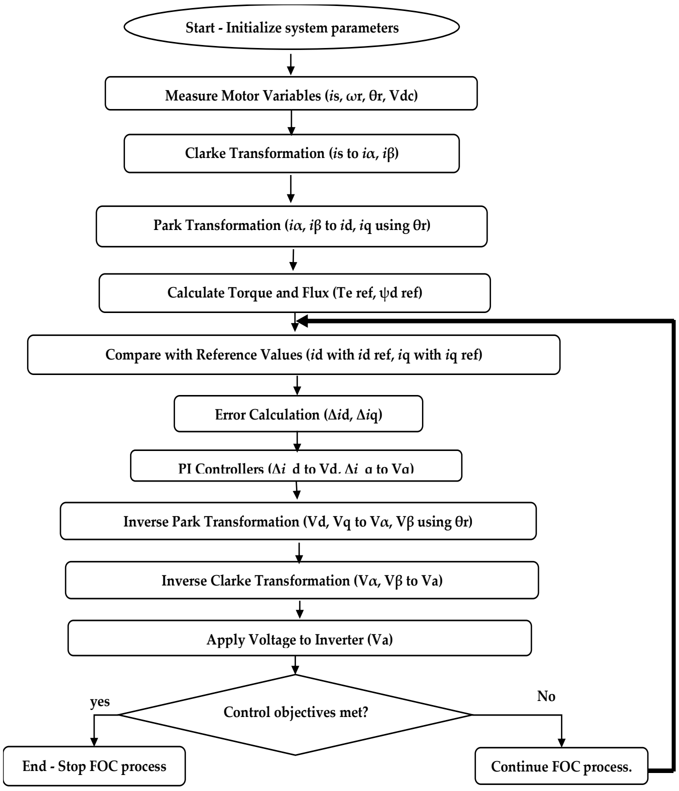

Figure 5. FOC controller (a) Architecture for 1-Ø Induction Motor (b) FOC flowchart

4.2 The 1-Ø Induction Motor with DTC Technique

DTC technology guarantees high economy and precise and quick torque dynamics. The direct application of a control sequence to upstream voltage inverter switches (switching states) is the main goal of the DTC concept [29]. A switching table, two hysteresis regulators, and the machine's electromagnetic torque and flux decoupling are progressively controlled and regulated[3]. *Figure 6(a)* depicts a simple DTC control structure [30], and *figure 6(b)* depicts a flowchart for DTC algorithm. A three-level hysteresis comparator is used to control electromagnetic torque.

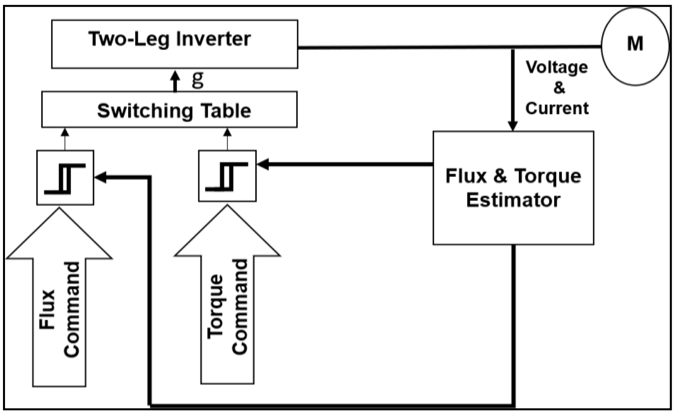

(a)

FOREX Publication
Open Access | Rapid and quality publishing
International Journal of
Electrical and Electronics Research (IJEER)
Research Article | Volume 12, Issue 3 | Pages 827-835 | e-ISSN: 2347-470X

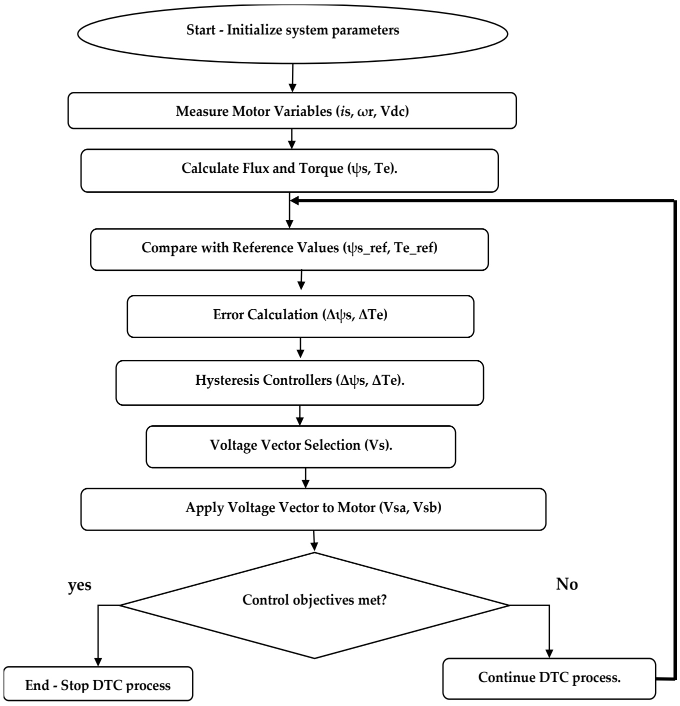

Figure 6. DTC controller (a) DTC Architecture for 1-Ø Machine (b) DTC flowchart

The stator flow is altered via an adjustable two-level hysteresis comparator. According to [21], the switching table is generated using the results of these comparators and the flow vector's information. The following formulas [21] are utilized to calculate the electromagnetic torque T_{em} and the stator flux $\emptyset_s$ in the DTC:

$$\emptyset_{s\alpha} = \int_0^t (v_{s\alpha} - R_s . i_{s\alpha}). dt \quad (9)$$

$$\emptyset_{s\beta} = \int_0^t (v_{s\beta} - R_s . i_{s\beta}). dt \quad (10)$$

Where $\emptyset_{s\alpha}$ and $\emptyset_{s\beta}$ are the stator α and β axis flux linkages, $v_{s\alpha}$ and $v_{s\beta}$ are stator voltages and $R_s . i_{s\alpha}$ and $R_s . i_{s\beta}$ are voltage drops in stator resistance.

The flux linkage phasor magnitude $\emptyset_s$ and angle θ_s are:

$$\emptyset_s = \sqrt{\emptyset_{s\alpha}{}^2 + \emptyset_{s\beta}{}^2} \quad (11)$$

While, θ_s is calculated from:

$$\theta_s = \tan^{-1} \frac{\emptyset_{s\beta}}{\emptyset_{s\alpha}} \quad (12)$$

$$T_{em} = p.(\emptyset_{s\alpha} . i_{s\beta} - \emptyset_{s\beta} . i_{s\alpha}) \quad (13)$$

After that, the results are sent into the hysteresis comparators, which compare the estimated stator flux and electromagnetic torque values with the respective reference values T_{em}* and s* [22]. The control table chooses the proper voltage vector, as seen in [23]. The table's inputs are the hysteresis comparator outputs and the flux sector number [24].

5. SIMULATION RESULTS & DISCUSSION

Under various PV array conditions, the simulation program "MATLAB" A single induction motor's performance and characteristics were evaluated. The results were obtained by varying three distinct temperature degrees' worth of light. By displaying the electromagnetic torque *Te* and Speed of the motor, the findings are taken in response to the employment of two controlling techniques for the drive system: FOC and DTC.

5.1 Simulation Result of PV Array

The V-I & V-P characteristics of Trina solar TSM-250PA05.08 array type is demonstrated in *figures 7* and *8* for three levels. The V-I characteristics at the utilization of the FOC controller for the array at 25° with specified irradiation is illustrated in *figure 7(a)*, while that for 1000 W/m^2 and specified temperature is illustrated in *figure 7(c)*. The V-I characteristics at the utilization of the DTC controller for the array at 25° with specified irradiation are illustrated in *figure 7(b)*. In contrast, those for 1000 W/m2 and specified temperature are illustrated in *figure 7(d)*. By comparing the results obtained for the V-I characteristics for both FOC & DTC, the results show agreement between the two curves for the generated current (In each cases current is 8.55 ampere).

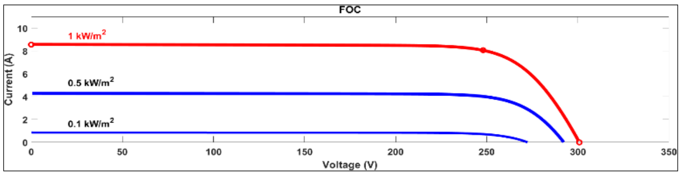

(a) Array @ 25° & specified irradiance for FOC

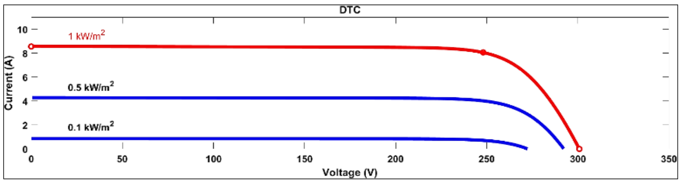

(b) Array @ 25° & specified irradiance for DTC

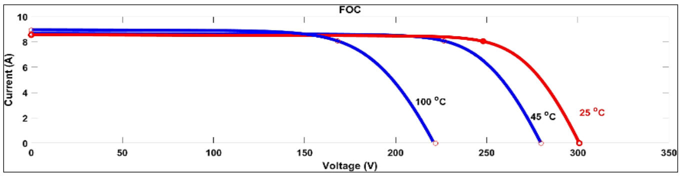

(c) Array @ 1000 W/m2 & specified temperature for FOC

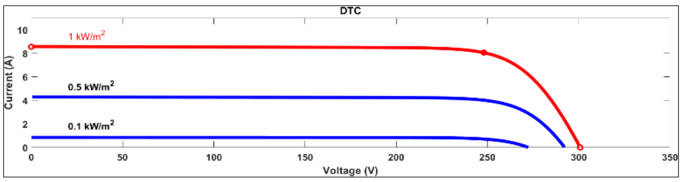

(d) Array @ 1000 W/m2 & specified temperature for DTC

Figure 7. V-I characteristics of Trina solar TSM-250PA05.08 array type

Research Article | Volume 12, Issue 3 | Pages 827-835 | e-ISSN: 2347-470X

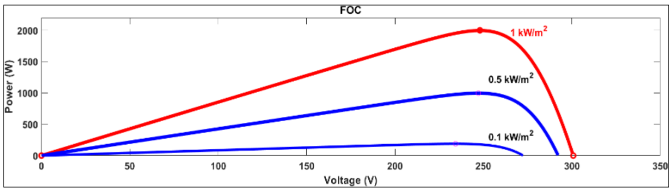

(a) Array @ 25○ & specified irradiance for FOC

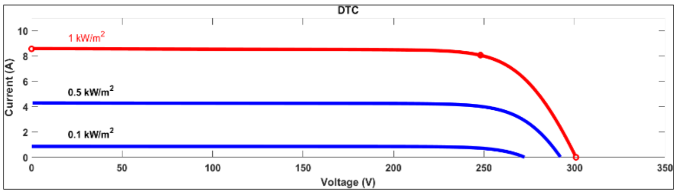

(b) Array @ 25○ & specified irradiance for DTC

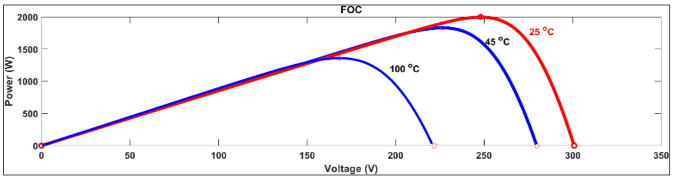

(c) Array @ 1000 W/m2 & specified temperature for FOC

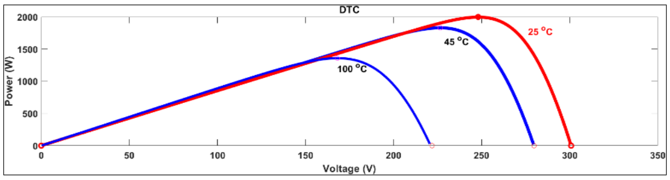

(a) Array @ 1000 W/m² & specified temperature for DTC

Figure 8. V-P characteristics of TSM-250PA05.08 array

The P-V characteristics at the utilization of the FOC controller for the array at 25° with specified irradiation is illustrated in *figure 8(a)*, while that for 1000 W/m² and specified temperature is illustrated in *figure 8(c)*. The P-V characteristics at the utilization of the DTC controller for the array at 25° with specified irradiation are illustrated in *figure 8(b)*. In contrast, those for 1000 W/m2 and specified temperature are illustrated in *figure 8(d)*. By comparing the results obtained for the P-V characteristics for both FOC & DTC, the results show agreement between the two curves for the generated power (maximum power generated for the array is 1998.88 watts at 284 volts in each case).

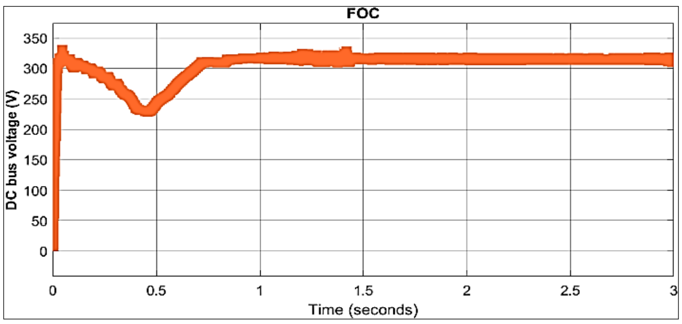

(a) For FOC

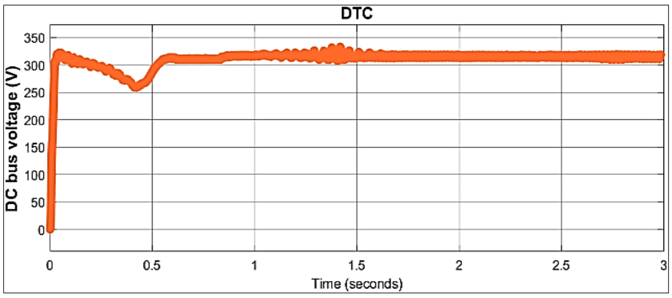

(b) For DTC

Figure 9. DC voltage waveform at utilizing: (a) FOC controller (b) DTC controller

The DC voltage waveform produced when FOC is used is shown in *figure 9(a)*, and the DC voltage waveform for DTC is shown in *figure 9(b)*.

5.2 Simulation Results of 1-Ø Induction Motor.

The simulation's outcomes for a 1-Ø induction motor demonstrate a strong association with the factors controlling variations in sun irradiation. The results are considered by electromagnetic torque (*Te*), motor rotor speed, and main and auxiliary winding currents (*Ia* & *Ib*, respectively), displaying the system's responsiveness to FOC and DTC. *Table 3* contains simulation results for Settling and rise time for torque and currents (main *Ias* and auxiliary *Ibs*). *Table 3* shows that the DTC response outperforms the FOC response regarding settling time.

Table 3. Settling time and Rise time results for FOC and DTC

Controller type	**FOC**	**DTC**
Settling time	20 ms	19.975 ms
Rise time		
Electromagnetic torque	2.475 ms	475.658 µs
Main winding current	2.796 ms	3.964 ms
Auxiliary winding current	270.995 µs	58.21 µs
DC voltage by PV	331.8 volt	330 volts

Regarding response time, the FOC main current was more responsive than the DTC main current; nevertheless, the DTC auxiliary current and DC voltages in the solar cells were superior to the FOC ones. The results of studies using the approach on the same system under identical climatic circumstances affecting solar cells support the claim that the DTC method is superior to the FOC. *Figures 10 (a)* and *10(b)* show the induction motor's rotor speed, correctly matching its FOC and DTC reference values. Both FOC and DTC exhibit steady-state speed characteristics between 1.5 and 2 seconds. This indicates that the systems reach and maintain a stable speed within this time frame.

FOREX Publication
Open Access | Rapid and quality publishing
International Journal of
Electrical and Electronics Research (IJEER)
Research Article | Volume 12, Issue 3 | Pages 827-835 | e-ISSN: 2347-470X

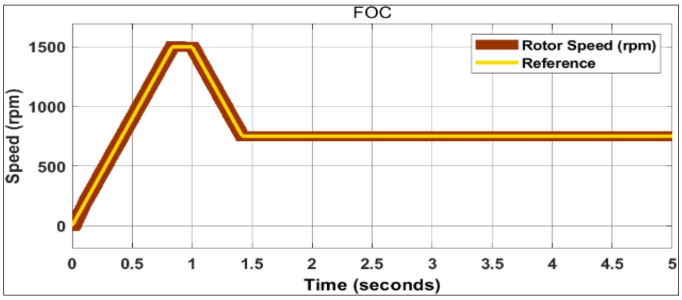

(a) FOC

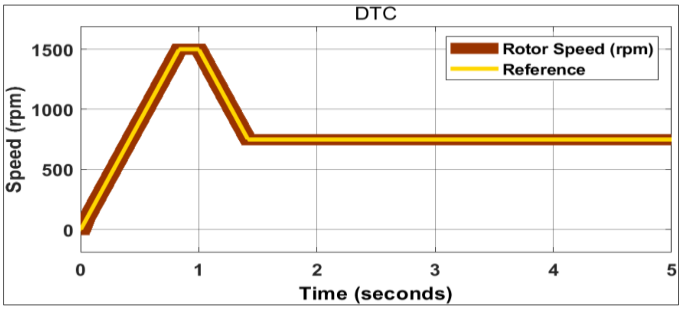

(b) DTC

Figure 10. Rotating Speed:(a) FOC (b)DTC

The main winding currents *Ia* and auxiliary winding currents *Ib* impacted by both approaches are depicted in *figures 11(a)* & *11(b)*. The currents still exhibit variations during the steady-state period (1.5-2 seconds). This suggests that while the speed is stable, the current dynamics are adjusting to maintain this steady speed. These adjustments are due to the control strategies responding to load changes or other disturbances.

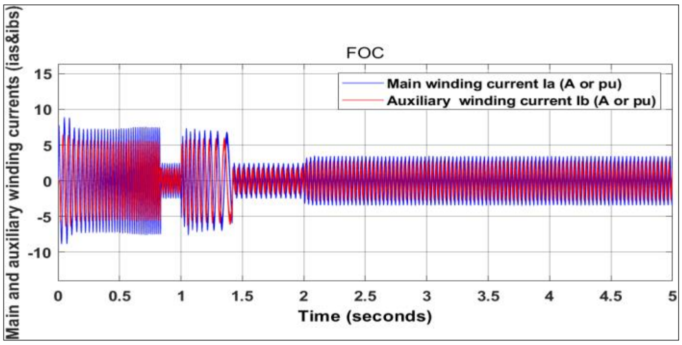

(a) FOC

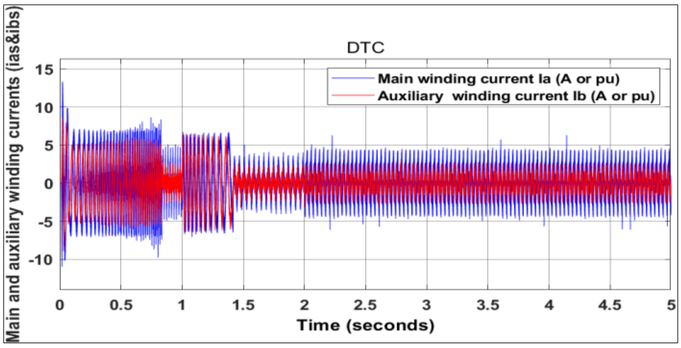

(b) DTC

Figure 11. Main and Auxiliary Winding Currents:(a) FOC (b)DTC

Figures 12(a) and *12(b)* demonstrate the *Te* for both FOC and DTC with a long settling time of two seconds. The torque shows changes even during the steady-state speed period. This variation in torque is necessary to compensate for any disturbances or to maintain the desired speed, reflecting the active role of the control strategies in managing the torque to achieve stable operation. FOC uses negative torque to decelerate and stabilize the motor, ensuring smooth and controlled operation. DTC frequently generates negative torque due to rapid switching of voltage vectors, managing dynamic changes effectively but with more torque ripple compared to FOC.

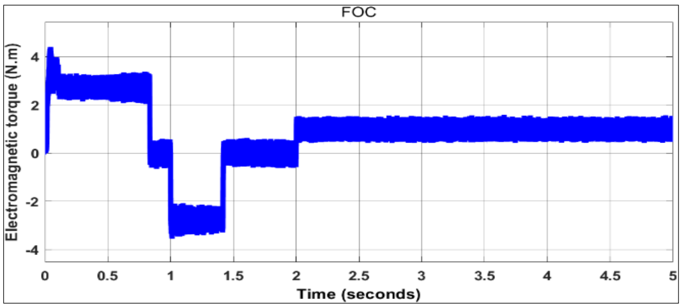

(a) FOC

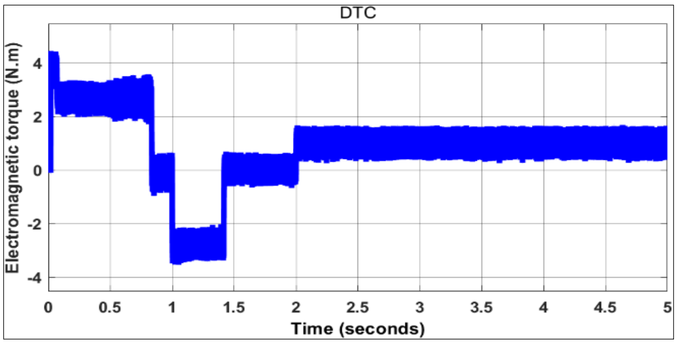

(b) DTC

Figure 12. Electromagnetic Torque Te: (a) FOC (b)DTC

6. CONCLUSIONS

According to this study, a single induction motor may be powered by Trina Solar's TSM-250PA05.08. MPP in the PV array was tracked using the P & O method. FOC and DTC are two control methods used and contrasted in 1-Ø induction motor. The results show how the 1-Ø induction motor reacts to a change in the step input while still responding well to changes in the main and auxiliary winding currents (*Ia* & *Ib*, respectively), torque (*Te*), and rotor speed. When comparing the FOC findings with the DTC results, numerous variations might be seen: (*i*)The DTC control technique demonstrated the presence of distortions in the main winding I_a and auxiliary winding I_b currents compared to the FOC control method results that demonstrate smoother waveform for I_a and I_b. (*ii*) The torque and Speed of the rotating portion were comparable for the two control methods (FOC & DTC). (*iii*) Regarding response time, DTC achieves faster rise time for both *Te* and *Ib*. (*iv*) Regarding settling time, DTC achieves faster rise time than FOC. (*v*) The steady-state speed achieved between 1.5-2 seconds and the continuous changes in torque and currents during this period reflect the system's response to external factors and the effectiveness of the FOC and DTC methods in stabilizing the motor's performance.

Author Contributions: 1. Suha Sabah Shyaa.; methodology, investigation, writing—original draft preparation. 2. Nihad Abdulkudhur Jasim; writing—review and editing. authors have read and agreed to the published version of the manuscript.

REFERENCES

[1] M. N. Almani, G. A. Hussain, and A. A. Zaher, "An Improved Technique for Energy- Efficient Starting and Operating Control of Single-Phase Induction Motors," IEEE Access, vol. 9, pp. 12446–12462, 2021, https://doi: 10.1109/ACCESS.2021.3050920.

[2] I. D. Chasiotis, Y. L. Karnavas, and F. Scuiller, "Effect of Rotor Bars Shape on the Single-Phase Induction Motors Performance: An Analysis toward Their Efficiency Improvement," Energies, vol. 15, no. 3, 2022, https://doi: 10.3390/en15030717.

[3] M. M. Alshbib, I. M. Alsofyani and M. M. Elgbaily, "Enhancement and Performance Analysis for Modified 12 Sector-Based Direct Torque Control of AC Motors: Experimental Validation," Electronics (Switzerland), vol. 12, no. 3, 2023. https://doi.org/10.3390/electronics1203054.

[4] Y. N. I. Alothman, W. E. Abdul-Lateef and S. A.-H. Gitaffa, "Using sensorless direct torque with fuzzy proportional-integral controller to control three phase induction motor," Bulletin of Electrical Engineering and Informatics, vol. 12, no. 2, pp. 738-748, 2023. https://doi: 10.11591/eei.v12i2.3991.

[5] J. Zhu, X. Wang, B. Xu, H. Feng and X. Xu, "A comparative study on field-oriented control and direct torque control for permanent magnet linear synchronous motor," Journal of Computers (Finland), vol. 8, no. 1, pp. 256-263, 2013. https://doi: 10.4304/jcp.8.1.256-263.

[6] S. S. Shyaa, N. A. Jasim, Y. H. Takheal and D. N. Mahdy, "Operation and control of a 1-Φ induction machine fed from a typical transformer-less photovoltaic (PV) cells," International Journal of Power Electronics and Drive Systems, vol. 14, no. 2, pp. 754-761, 2023. https://doi: 10.11591/ijpeds.v14.i2.pp754-761.

[7] N. Maleki, M. R. A. Pahlavani and I. Soltani, "A Detailed Comparison Between FOC and DTC Methods of a Permanent Magnet Synchronous Motor Drive," Journal of Electrical and Electronic Engineering, vol. 3, no. 2, pp. 92-100, 2015. https://doi: 10.11648/j.jeee.s.2015030201.30.

[8] O. C. Sekhar and S. Lakhimsetty, "Direct torque control scheme for a five-level multipoint clamped inverter fed induction motor drive using fractional-order PI controller," International Transactions on Electrical Energy Systems, vol. 30, no. 9, pp. 1-24, 2020. https://doi.org/10.1002/2050-7038.12474.

[9] M. El Mahfoud, B. Bossoufi, N. El Ouanjli, M. Said and M. Taoussi, "Improved Direct Torque Control of Doubly Fed Induction Motor Using Space Vector Modulation," International Journal of Intelligent Engineering and Systems, vol. 14, no. 3, pp. 177-188, 2021. https:// doi:10.22266/ijies2021.0630.16.

[10] M. J. B. Kabeyi and O. A. Olanrewaju, "Sustainable Energy Transition for Renewable and Low Carbon Grid Electricity Generation and Supply," Frontiers in Energy Research, vol. 9, no. March, pp. 1-45, 2022. https:// doi: 10.3389/fenrg.2021.743114.

[11] M. J. B. Kabeyi and O. A. Olanrewaju, "Geothermal wellhead technology power plants in grid electricity generation: A review," Energy Strategy Reviews, vol. 39, pp. 1-27, 2022. https://doi.org/10.1016/j.esr.2021.100735.

[12] S. Lekhchine, T. Bahi, I. Abadlia and H. Bouzeria, "PV-battery energy storage system operating of asynchronous motor driven by using fuzzy sliding mode control," International Journal of Hydrogen Energy, vol. 42, no. 13, pp. 8756-8764, 2017. https:// doi: 10.1016/j.ijhydene.2016.05.298.

[13] M. Calavia, J. M. Perié, J. F. Sanz and J. Sallán, "Comparison of MPPT strategies for solar modules," Renewable Energy and Power Quality Journal, vol. 1, no. 8, pp. 1440-1445, 2010. https:// doi:10.24084/repqj08.685.

[14] B. Singh, U. Sharma and S. Kumar, "Standalone Photovoltaic Water Pumping System Using Induction Motor Drive with Reduced Sensors," IEEE Transactions on Industry Applications, vol. 54, no. 4, pp. 3645-3655, 2018. https:// doi: 10.1109/TIA.2018.2825285.

[15] A. K. Saini and A. K. Dubey, "Performance Analysis of Single-Phase Induction Motor with Solar PV Array for water Pumping System," International Journal of Engineering Research and Technology, vol. 6, no. 4, pp. 721-727, 2017. https:// doi: 10.17577/ijertv6is040567.

[16] C.-E. Feraga and A. Bouldjedri, "Perfomanse fotonaponskog sustava pumpanja pogonjenog jednofaznim indukcijskim motorom spojenim na fotonaponski generator," Automatika, vol. 57, no. 1, pp. 163-172, 2016. https:// doi:10.22266/ijies2021.0630.16.

[17] D. E. Tourqui, A. Betka, A. Smaili and T. Allaoui, "Improved Performance of a Photovoltaic Panel by MPPT Algorithms," in Recent Developments in Photovoltaic Materials and Devices, intechopen., 2019, pp. 65-84. https:// doi: 10.5772/intechopen.79709.

[18] M. Y. Javed, A. F. Mirza, A. Hasan, S. T. H. Rizvi, Q. Ling, M. M. Gulzar, M. U. Safder and M. Mansoor, "A comprehensive review on a PV based system to harvest maximum power," Electronics (Switzerland), vol. 8, no. 12, pp. 1-68, 2019. https:// doi:10.3390/electronics8121480.

[19] A. Anurag, S. Bal, S. Sourav and M. Nanda, "A review of maximum power-point tracking techniques for photovoltaic systems," International Journal of Sustainable Energy, vol. 35, no. 5, pp. 478-501, 2019. https://doi.org/10.1080/14786451.2014.918979.
[20] S. Bandri, Zulkarnaini, A. Syofian and . A. AEffendi, "The application of perturb and observe algorithm to optimized of solar cell output," 2019. https://doi:10.1088/1742-6596/1185/1/012012.

[21] B. Subudhi and R. Pradhan, "A comparative study on maximum power point tracking techniques for photovoltaic power systems," IEEE Transactions on Sustainable Energy, vol. 4, no. 1, pp. 89-98, 2013. https:// doi: 10.1109/TSTE.2012.2202294.

[22] M. Jannati, T. Sutikno, N. Idris and M. Aziz, "A novel method for rotor field-oriented control of single-phase induction motor," International Journal of Electrical and Computer Engineering, vol. 5, no. 2, pp. 205-212, 2015. http://doi.org/10.11591/ijece.v5i2.pp205-212.

[23] M. Jannati, S. A. Anbaran, S. H. Asgari, W. Y. Goh, A. Monadi, M. J. Abdul Aziz and N. R. N. Idris, "A review on Variable Speed Control techniques for efficient control of Single-Phase Induction Motors: Evolution, classification, comparison," Renewable and Sustainable Energy Reviews, vol. 75, no. july, pp. 1306-1319, 2017. https://doi.org/10.1016/j.rser.2016.11.115.

[24] K. J. Lee, H. G. Kim, D. K. Lee, T. W. Chun and E. C. Nho, "High performance drive of single-phase induction motor," Korea, 2001. https:// doi:10.1109/isie.2001.931608.

[25] M. I. Rahman and K. M. Salim, "Performance evaluation of single-phase induction motor controlled by variable frequency drive at non-ideal voltage conditions," Australian Journal of Electrical and Electronics Engineering, vol. 16, no. 2, pp. 65-73, 2019. https://doi.org/10.1080/1448837X.2019.1600213.

[26] N. T. Pham and K. H. Nguyen, "Sensorless control for high performance SPIM drives based on the improved rotor flux identifier using sliding mode," International Journal of Intelligent Engineering and Systems, vol. 12, no. 4, pp. 291-305, 2019. https:// doi: 10.22266/ijies2019.0831.27.

[27] H. B. Azza, N. Zaidi, M. Jemli and M. Boussak, "Development and Experimental Evaluation of a Sensorless Speed Control of SPIM Using Adaptive Sliding Mode-MRAS Strategy," IEEE Journal of Emerging and

Selected Topics in Power Electronics, vol. 2, no. 2, pp. 319-328, 2014. https://doi: 10.1109/JESTPE.2014.2299893.

[28] N. T. Pham, D., P. Nguyen, K., H. Nguyen and N. V. Nguyen, "A novel Neural Network SC_MRAS based observer for high-performance SPIM drives," International Journal of Intelligent Engineering and Systems, vol. 11, no. 6, pp. 95-107, 2018. https:// doi: 10.22266/IJIES2018.1231.10.

[29] I. Saady, M. K. Karim, B. Bossoufi, N. E. Ouanjli, S. Motahhir and B. Majout, "Optimization and control of photovoltaic water pumping system using kalman filter based MPPT and multilevel inverter fed DTC-IM," Results in Engineering, vol. 17, no. December, pp. 1-14, 2023. https://doi.org/10.1016/j.rineng.2022.100829.

[30] R. . d. F. Campos, L. F. R. Pinto, J. d. Oliveira, A. Nied, u. C. d. S. Marques and A. D. ouza, "Single-phase induction motor control based on DTC strategies," IEEE International Symposium on Industrial Electronics, no. july, pp. 1068-1073, 2007. https://doi.org/10.1016/j.rineng.2022.100829.